Key Dynamics from a Simple Model of HIV Infection

Faustino Sánchez Garduño, Denise Kirschner
and Janelle Reynolds

Abstract. There have been many models to date describing the interaction of the immune system with HIV. Each presents some aspect or aspects of the immune system believed to play a key role in the disease dynamics. In this study, we again explore the immune interactions; however from a very basic perspective. Our focus is the key first order effects which are necessary for a model of HIV-immune interaction to explain the different stages of disease progression. Our model is a non-linear autonomous ODE system; dependent on several biological parameters. We analyze the global dynamics of the system for different sets of parameters varied within the proper parameter space. We also include numerical simulations of the relevant phase portraits.

§1. Introduction

Over the past decade a number of mathematical models have been developed to describe the interaction of the immune system with the human immunodeficiency virus (HIV). For example, see [4,5,6,8,9,10,11,12,14]. Different phenomenon are explained by the different models, but none of the models exhibit all of what is observed clinically. This is partly due to the fact that much about this disease's mechanics is still unknown. However, many of the major features can be simulated with even the simplest of models.

Thus, the main focus of the model we present is to explore the simplest mathematical descriptions of the interaction of HIV and the human immune system necessary to capture the first order effects seen clinically. Namely, the three major outcomes are: an uninfected state, where the body clears HIV (no infection present); an infected state, where the T cells and virus have high turnover rates on a daily basis, but the overall appearance is of a steady state with low levels of free virus in the blood and a significantly reduced T cell count (from normal which is approx. 1000 per mm^3); and then a progression to AIDS state, where the T cells significantly decline and the virus population

Mathematical Models in Medical and Health Sciences
Mary Ann Horn, Gieri Simonett, and Glenn Webb (eds.), pp. 161–196.

ISBN 0-8265-1310-7.

expands. The immunological understanding of these different stages of disease progression are still not well understood, but we hope to gain insight into the processes through the modeling endeavors.

In this work, we present a simple model for the interaction of the immune system with HIV and then carry out a non-dimensionalization. On this nondimensionalized version, we do an extensive global analysis using both numerical and analytical techniques to analyze the rich behavior arising in the dynamical system. Finally, we discuss the implications of mathematical results for the biological problem of HIV disease progression.

§2. The Model and Its Non-Dimensional Version

HIV destruction of the immune system works mainly by infecting CD4$^+$ T cells, the cells responsible for the governing of the immune system. Therefore, we create a model incorporating only these two populations and their interactions and effects. More detailed models incorporating different classes of cells and virus have been studied as well (e.g. [4,5,6,8,9,10,11,12,14,16]), but our aim is to create a simple model capturing the rich clinical behavior. Define $T(t)$ to be the CD4$^+$ T cell population at time t. Define $V(t)$ to be the free virus population at time t. We assume only one strain of virus. A simple model describing the interaction of HIV with the immune system is then as follows:

$$\frac{dT}{dt} = \sigma - \mu T(t) + T(t)\frac{pV(t)}{C+V(t)} - K_{V,T}T(t)V(t), \tag{1}$$

$$\frac{dV}{dt} = \hat{N} \cdot K_{V,T}T(t)V(t) - K_{T,V}T(t)V(t) + G_V V(t). \tag{2}$$

Initial conditions are $T(0) = T_0$, and $V(0) = V_0$. (We assume the initial innoculum is free virus and not infected cells.)

The model is explained as follows. The terms of (1), $\sigma + \frac{pV(t)}{C+V(t)}T(t)$, represent the source of new T cells. This incorporates T cells from the bone marrow, thymus and general production. It also includes proliferative production (whether direct or indirect) due to the presence of antigen. This production changes over the course of infection, which is accounted for in the choice of terms. This is followed by a natural death term, because cells have a finite life span; the average of which is $\frac{1}{\mu_T}$. The last term of (1) represents the infection of CD4$^+$ T cells by virus. This term is a mass action type term with constant rate of infectivity $K_{V,T}$. We assume the law of mass action applies here based on the large numbers of cells and virion involved. In (2), the first term is the source for the virus population. Newly produced virion are produced by infected CD4$^+$ T cells (hence it follows from (1)), whereby new virion are produced at the rate $\hat{N} \cdot K_{V,T}T(t)$. There is a high clearance rate of virus, on a daily basis, [14], and this is reflected in the next term $-K_{T,V}T(t)V(t)$. As there is much evidence to support the major production of virus taking place in the external lymphoid system (LS), we account for this phenomenon as a major contributor of virions, other than the small amount produced in the blood [7]. The input rates of lymphoid system virus is $G_V(t)$.

This is a simple possible model representing the interactions of T cells and virus. This model was studied in a 3 equation form (with a separate equation for the infected T cells) and the parameter values were all estimated there [4,5,6]. We summarize those results in Table 1, which gives a list of all parameters along with their estimated numerical values.

If we first examine the system for steady-state values, we find there are three possible steady states in the positive cone depending on the parameter space. Hence, we define the different steady states for the system as follows: *Uninfected steady state* (where the virus population and infected cells are $\bar{V} = 0$ and $\bar{T} = \frac{s}{\mu}$), and an *Infected Steady State* (both virus and T cells exist at some positive level). This corresponds to the extended latent period of the disease. Another limiting behavior for the system is *Progression to AIDS* (the T cell population goes to 0, and V grows without bound - which is consistent with the Center for Disease Control's definition for AIDS).

Before further analysis, we performed a non-dimensionalization. Define the new variables as:

$$T^{\text{new}} = T/T_{\max}, \quad V^{\text{new}} = V/C, \quad t^{\text{new}} = pt,$$
$$\frac{dT^{\text{new}}}{dt^{\text{new}}} = \frac{d(T/T_{\max})}{d(pt)} = \frac{\frac{1}{T_{\max}}}{p}\frac{dT}{dt}. \tag{3}$$

Substituting (3) into (1) and (2) and suppressing the "new"notation, the equations are transformed into:

$$\frac{dT}{dt} = s - mT + \frac{TV}{1+V} - k_1 VT, \tag{4}$$

$$\frac{dV}{dt} = NTV - k_2 VT + gV, \tag{5}$$

with

$$s = \frac{\sigma}{T_{\max} \cdot p}, \quad m = \frac{\mu}{p}, \quad k_1 = \frac{K_{V,T}K}{p} \quad N = \frac{\hat{N}K_{V,T}T_{\max}}{p},$$
$$k_2 = \frac{K_{T,V}T_{\max}}{p} \quad \text{and} \quad g = \frac{G_V}{p}.$$

One advantage of this new system (4-5) is that the number of parameters has been reduced from 9 to 6.

§3. The Phase Portrait Analysis

Define the right hand sides of (4-5) to be the functions $f_1(V,T)$ and $f_2(V,T)$, respectively, as shown:

$$\dot{V} = NTV - k_2 TV + gV \equiv f_1(V,T),$$
$$\dot{T} = s - mT + \frac{TV}{1+V} - k_1 TV \equiv f_2(V,T), \tag{6}$$

where all the parameters are positive.

Before we begin analysis of this system, we wish to point out a transformation. Let $V = e^x$ and $T = e^y$. Then this system is transformed into:

$$\dot{x} = -ke^y + g,$$
$$\dot{y} = se^{-y} - m + \frac{e^x}{(1+e^x)} - k_1 e^x.$$

This system is well-known from Lotka-Volterra theory. It is easy to show that the divergence of the vector field is $div = -se^{-y}$ which is always negative, thus by Bendixson's negative criterion, there are no periodic solutions, and all bounded trajectories converge. We will however, be concerned directly with the dynamical behavior of the phase portrait in the VT-plane, and what the implications are to the biological problem of HIV-T cell dynamics. Therefore, we will perform the remainder of the analysis on the original system given in (6). Future work could examine how our original VT-plane and trajectories are changed via this transformation. For example, the $V = e^x$ and $T = e^y$ transformation maps the positive orthant into the whole plane. It would be of interest to see how closed trajectories are mapped into closed trajectories, etc.

The dynamics of the system (6) depends strongly on the behavior of the nullclines. These are given by the set $\{(V,T) \mid f_1(V,T) = f_2(V,T) = 0\}$. The horizontal nullcline has two branches: $V \equiv 0$ and the horizontal line

$$T_{hor} = \frac{g}{k_2 - N} \equiv T^*. \tag{7}$$

Hereafter we will assume $(k_2 - N) > 0$, as negative cell populations do not make biological sense. The vertical nullcline is the graph of the function

$$T_{vert}(V) = \frac{s + sV}{k_1 V^2 + rV + m}, \tag{8}$$

where $r = m + k_1 - 1$. Note that $T_{vert}(0) = s/m$, $T_{vert}(-1) = 0$, $T_{vert}(V) \to 0$ as $V \to +\infty$ or as $V \to -\infty$.

Given that the vertical nullcline (8) depends on three parameters: k_1, m and s, its geometric features will also depend on them; particularly, whether or not the denominator, $D(V)$,

$$D(V) = k_1 V^2 + rV + m, \tag{9a}$$

has roots. If they exist, the roots of $D(V)$ are

$$V_1, V_2 = \frac{-r \pm \sqrt{r^2 - 4k_1 m}}{2k_1}. \tag{9b}$$

Clearly, the signs of V_1 and V_2 are of concern for biological feasibility as well. Let us write the discriminant, $d = r^2 - 4k_1 m$, explicitly

$$d = [(m - k_1)^2 - 2(m + k_1) + 1]. \tag{10}$$

We note that in the mk_1-parameter plane the graphs of the functions

$$k_1^1(m) = (1+m) + 2\sqrt{m} \quad \text{and} \quad k_1^2(m) = (1+m) - 2\sqrt{m} \tag{11}$$

are the boundaries between the regions on which the function $D(V)$ has none or two real roots, corresponding to $d < 0$ and $d > 0$, respectively. Figure 1 illustrates the space of the parameters in the mk_1-plane.

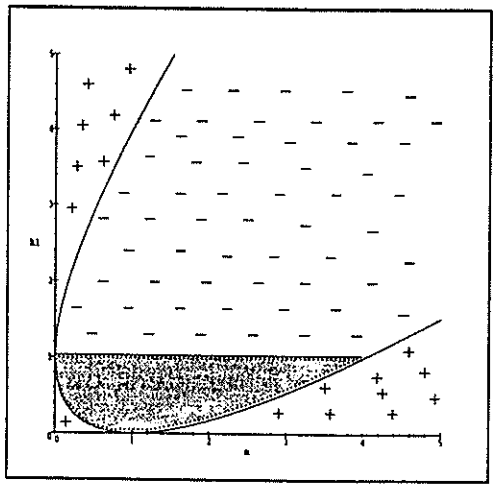

Fig. 1. Space parameters for the roots of $D(V) = k_1V^2 + rV + m$. On the region (+) D has two real roots, on (−) there are not real roots and on the graph of k_1^1 and k_1^2, D has one real root.

Depending on the sign of d we will divide the analysis in three major cases. Case 1 is $d < 0$; Case 2 is $d = 0$; and Case 3 is $d > 0$. The results are summarized in Table 2 and the analysis follows in the next subsections.

3.1. Phase Portrait Analysis in Case 1:

$$d = [(m-k_1)^2 - 2(m+k_1) + 1] < 0.$$

Here the function $D(V)$, (9a), has no real roots. This situation corresponds to the region marked with negative (−) signs in Figure 1, i.e.

$$m + 1 - 2\sqrt{m} < k_1 < m + 1 + 2\sqrt{m}. \tag{12}$$

First we need to determine the qualitative profile of T_{vert} (8). One can verify that, provided $[k_1V^2 + (m + k_1 - 1)V + m] \neq 0$, T_{vert} has a maximum at $V = \tilde{V}_1 = -1 + 1/\sqrt{k_1}$ whose value is $T_{vert}(\tilde{V}_1) = s/(2\sqrt{k_1} + m - k_1 - 1)$ and one minimum at $V = \tilde{V}_2 = -1 - 1/\sqrt{k_1}$ whose value is $T_{vert}(\tilde{V}_2) = s/(m - 1 - 2\sqrt{k_1} - k_1)$. For the set of parameters m and k_1 given in (12), $T_{vert}(\tilde{V}_1) > 0$ and $T_{vert}(\tilde{V}_2) < 0$.

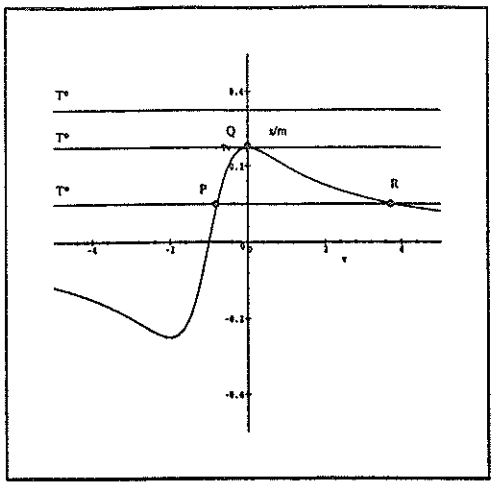

Fig. 2. Case **1.a.i**: $d < 0$. There are at most three steady states as the value of $T^* = T_{hor}$ varies.

Depending on the value of the parameters, providing the inequality (12) holds, we have three Sub-Cases.

Before the phase portrait analysis we first define the region of biological interest, namely

$$\Omega = \{(V,T) \mid 0 \leq V < \infty; 0 \leq T < \infty\}.$$

Case 1.a: $k_1 = 1$.

Here $\widetilde{V}_1 = 0$ and $\widetilde{V}_2 = -2$. The condition $d = [(m - k_1)^2 - 2(m + k_1) + 1] < 0$, implies $0 < m < 4$. In addition we have $T_{vert}(0) = s/m = \max T_{vert}(V) \equiv M$. For the parameter values in Table 1, the value of $M = \frac{1}{3}$ in this scaled form. The graph of T_{vert} is the curve shown in Figure 2. Depending on T^*, we have there possible cases (see Figure 2):

i) $0 < T^* < M$. Here the system (6) has three equilibria: P, Q and R. Given the biological interpretation of the variables, the point P is not feasible.

ii) $T^* = M$. Here the points P and R collapse into Q, thus the system (6) has only one equilibrium: Q.

iii) $T^* > M$. Here the nullclines have no intersection. Thus the system (6) has one equilibrium point: Q.

Now we will determine the qualitative behavior of the trajectories of (6) for each one of the above cases. Particularly we will focus on the existence of trajectories of (6) connecting pairs of equilibria (when it makes sense) i.e. on the existence of heteroclinic trajectories of (6).

Case 1.a.i.

The coordinates, (V^*, T^*), of the equilibrium R are $T^* = \frac{g}{k_2 - N}$ and V^* is the positive root of

$$T^* V^2 + (mT^* - s)V + T^* m - s = 0, \tag{13}$$

i.e.

$$V^* = \frac{-(mT^* - s) + \sqrt{(mT^* - s)^2 - 4T^*(T^* m - s)}}{2T^*}. \tag{14}$$

This results from the condition $T^* < s/m$. The other equilibrium is Q. Our analysis starts by considering the local phase portrait of (6) around each equilibrium. Thus the Jacobian matrix of (6) at all points (V, T) is given by

$$\begin{aligned} J[f_1, f_2]_{(V,T)} &= \begin{bmatrix} \frac{\partial f_1}{\partial V} & \frac{\partial f_1}{\partial T} \\ \frac{\partial f_2}{\partial V} & \frac{\partial f_2}{\partial T} \end{bmatrix}_{(V,T)} \\ &= \begin{bmatrix} NT - k_2 T + g & NV - k_2 V \\ -\frac{VT(2+V)}{(1+V)^2} & \frac{-m - mV - V^2}{(1+V)} \end{bmatrix}. \end{aligned} \tag{15}$$

Evaluating (15) at Q we obtain

$$J[f_1, f_2]_{(0,s/m)} = \begin{bmatrix} \frac{s}{m}(N - k_2) + g & 0 \\ 0 & -m \end{bmatrix}, \tag{16}$$

which implies the trace is: $tr(J[f_1, f_2](0, s/m)) = \frac{s}{m}(N - k_2) + g - m$ and the determinant is $det\ J[f_1, f_2]_{(0,s/m)} = s(k_2 - N) - mg$. Because of the condition $T^* = \frac{g}{(k_2 - N)} < \frac{s}{m}$, $det\ J[f_1, f_2]_{(0,s/m)} > 0$ and $tr(J[f_1, f_2]_{(0,s/m)}) < 0$. Since the roots of the characteristic polynomial $\mathcal{P}(\lambda) = \left[\frac{s}{m}(N - k_2) + g - \lambda\right](-m - \lambda)$, of (16) are λ_1 and λ_2,

$$\lambda_1 = \left[\frac{s}{m}(N - k_2) + g\right] < 0 \quad \text{and} \quad \lambda_2 = -m < 0.$$

Then Q is a locally asymptotically stable node. Given that the element $a_{12} = 0$ in the Jacobian matrix (16), then except for the trajectory approaching Q through the line spanned by the eigenvector $\vec{v_2} = (\lambda_1, \lambda_2)^T$, all the trajectories of (6) tend to Q tangential to the vertical axis. Moreover, in a neighborhood of Q, the variables T and V are related by the equality

$$T(V) = aV^{\lambda_2/\lambda_1},$$

where a is any real number.

Now we evaluate (15) at $R = (V^*, T^*)$, from which we have

$$tr(J[f_1, f_2]_{(V^*,T^*)}) = \frac{-m - mV^* - V^{*2}}{(1 + V^*)} < 0, \text{ and}$$

$$det\ J[f_1, f_2]_{(V^*,T^*)} = -\frac{V^{*2} g(2 + V^*)}{(1 + V^*)^2} < 0.$$

Thus R is a hyperbolic saddle point.

The characteristic polynomial has the following roots:

$$\lambda_1, \lambda_2 = -\frac{(m + mV^* + V^{*2}) \pm \sqrt{(m + mV^* + V^{*2})^2 + 4gV^{*2}(2 + V^*)}}{2(1 + V^*)},$$

with $\lambda_1 > 0$ and $\lambda_2 < 0$. The eigenvectors corresponding to each eigenvalue are

$$\vec{v}_1 = (1 + p_1^2)^{-1/2} \begin{bmatrix} 1 \\ p_1 \end{bmatrix} \quad \text{and} \quad \vec{v}_2 = (1 + p_2^2)^{-1/2} \begin{bmatrix} 1 \\ p_2 \end{bmatrix},$$

where

$$p_1 = \frac{\lambda_1}{(N - k_2)V^*} < 0 \quad \text{and} \quad p_2 = \frac{\lambda_2}{(N - k_2)V^*} > 0.$$

The local phase portrait of (6) around Q and R is illustrated in Figure 3.

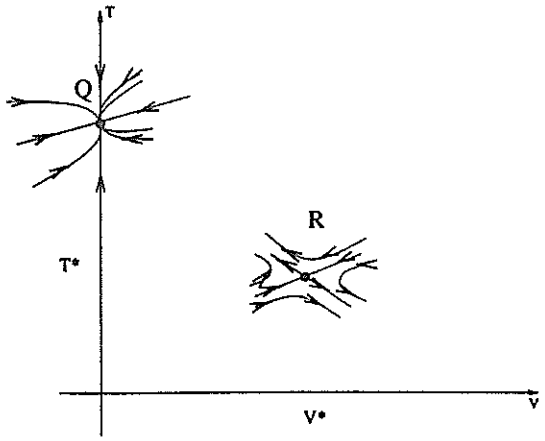

Fig. 3. Local phase portrait of (6) for the Sub-Case **1.a.i** with $0 < T^* < M$. Notice that Q is the locally asymptotic stable node and R is the saddle point.

Now we will determine the global behavior of the trajectories of (6) in the region of biological interest, namely Ω. First, note that the vector field defined by (6) is as in Figure 4(a). Second, note the left unstable manifold of (6), $W^u(R)$, at R leaves this equilibrium below the graph of the nullcline with slope $M^u(R) = \frac{\lambda_1}{(N-k_2)V^*} < 0$. Once $W^u(R)$ leaves R, the vector field (6) pushes it towards the shaded region $\mathcal{R}$ of Figure 4(b). Again, because of the vector field, this trajectory never goes outside of the region $\mathcal{R}$ as time increases. Moreover, given that

$$\frac{\partial f_1}{\partial V} + \frac{\partial f_2}{\partial T} = \left[(N - k_2)T + g - \frac{m - mV - V^2}{(1 + V)}\right] < 0 \qquad \forall\, (V, T) \in \mathcal{R},$$

then, by the Dulac's Test, the system (6) has no closed trajectory there. Since the system (6) has an equilibrium in $\mathcal{R}$, thus by the Poincaré-Bendixon Theorem [3], $W^u(R)$ must end at Q as time t goes to infinity.

This proof can be now summarized in the following proposition:

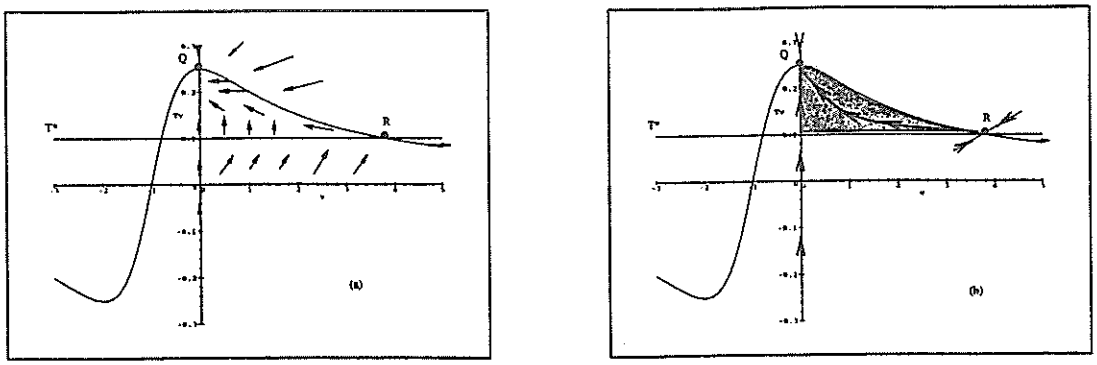

Fig. 4. Global behavior of the trajectories of (6) for the Case **1.a.i:** (a) Vector Field. (b) The trajectory $W^u(R)$ approaches Q as $t \to +\infty$.

Proposition 1.1. *For $k_1 = 1$ and for each m such that $0 < m < 4$ with $\frac{g}{k_2 - N} < \frac{s}{m}$, the trajectory $W^u(R)$ tends to Q as $t \to +\infty$.*

Case 1.a.ii.

Here $T^* = \frac{s}{m} = \frac{g}{k_2 - N}$ and the system (6) has just one equilibrium: $Q = (0, s/m)$. The Jacobian matrix (15) yields the $tr(J[f_1, f_2]_{(0,s/m)}) = -m < 0$ and $det\ J[f_1, f_2]_{(0,s/m)} = 0$. Thus, the equilibrium Q is a *non-hyperbolic* point of *co-dimensionone* i.e., the Jacobian has eigenvalues $\lambda_1 = 0$ and $\lambda_2 = -m$. The corresponding eigenvectors are $\vec{v}_1 = (m, 0)^T$ and $\vec{v}_2 = (0, 1)^T$, respectively.

According to the Centre Manifold Theorem [1], the system (6)

i) has a unique one-dimensional invariant stable manifold locally tangent to the eigenvector $\vec{v}_2$,
ii) has a one-dimensional invariant center manifold locally tangent to the eigenvector $\vec{v}_1$,
iii) except on the stable manifold, all other trajectories tend to the center manifold.

More detailed qualitative information on the local phase portrait of (6) around Q can be obtained by calculating an approximation to the center manifold of (6) at Q. (According with theorems from [1] this approximation of the center manifold of the normal form of the non-linear approximation of (6) at Q can be obtained with a sufficient degree of accuracy.) For this we need higher order terms in the Taylor Series, but for our present purpose, we do not need these technical details. It is enough to say that Q is a *saddle-node bifurcation point* and that the trajectories of (6) leaving Q through the center manifold travels away from Q tending to $(\mp\infty, 0)$ as time t increases. This follows from the vector field of (6). The phase portrait for this Sub-Case is shown in Figure 5.

The above analysis can be stated as the following proposition:

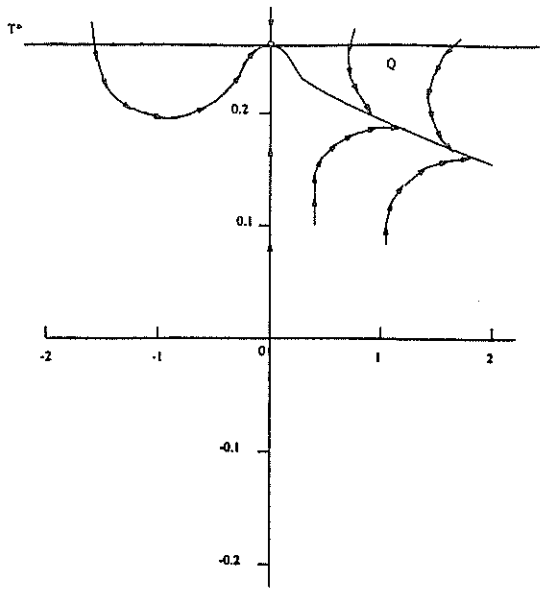

Fig. 5. Case **1.a.ii:** The saddle-node bifurcation point. The center manifold of (6) at Q runs away to $(\infty, 0)$, as $t \to +\infty$.

Proposition 1.2. *For $k_1 = 1$, $0 < m < 4$ and $\frac{s}{m} = \frac{g}{k_2 - N}$, the system (6) has a unique equilibrium point of saddle-node bifurcation type. Moreover the trajectory of (6) leaving Q through the center manifold tends to $(+\infty, 0)$ as $t \to +\infty$.*

Case 1.a.iii: $T^* > \frac{S}{m}$.

Here the system (6) has just one equilibrium: Q. The Jacobian matrix at Q yields:

$$det(J[f_1, f_2]_{(0,s/m)}) = -m\left[\frac{s}{m}(N - k_2) + g\right], tr(J[f_1, f_2]_{(0,s/m)})$$
$$= \frac{s}{m}(N - k_2) + g - m. \tag{17}$$

Because of the condition $\frac{g}{(k_2 - N)} > \frac{s}{m}$, we have $det\ J[f_1, f_2]_{(0,s/m)} < 0$, thus Q is a saddle point. The eigenvalues are $\lambda_1 = \left[\frac{s}{m}(N - k_2) + g\right] > 0$ and $\lambda_2 = -m < 0$. The stable manifold is on the vertical axis, while the unstable manifold has (at Q) a tangent vector (λ_1, λ_2). Again, because of the vector field, the unstable manifold of (6) at Q goes away from Q and tends to $(+\infty, 0)$ as $t \to +\infty$. Figure 6 illustrates the phase portrait.

We have proved the following proposition for Case (iii):

Proposition 1.3. *If $k_1 = 1$, $0 < m < 4$ and $\frac{g}{(k_2 - N)} > \frac{s}{m}$, the system (6) has only one equilibrium point which is a hyperbolic saddle point. The right unstable manifold of (6) tends to $(+\infty, 0)$ as $t \to +\infty$.*

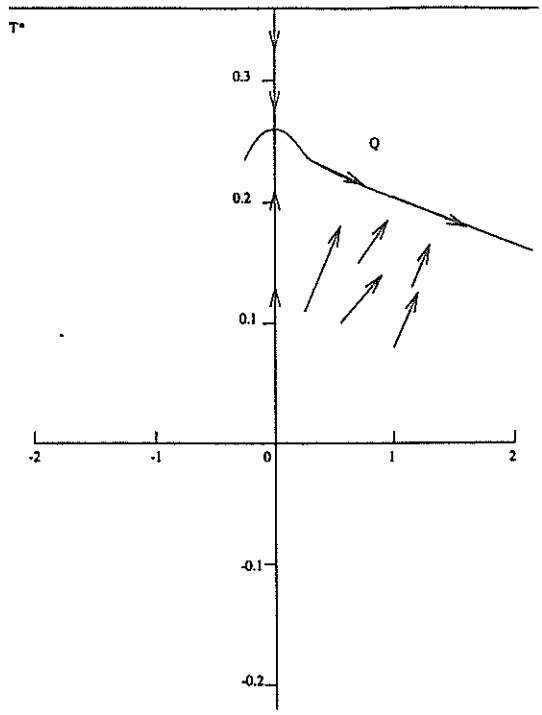

Fig. 6. Case **1.a.iii:** The unstable manifold at Q.

Case 1.b: $m+1-2\sqrt{m} < k_1 < 1$ with $0 < m < 4$.

Here the qualitative behavior of T_{vert} is illustrated in Figure 7 which also shows the different locations of T^*. There are rich dynamics in this Case.

Let $\max T_{vert}(V)$ be the maximum value of T_{vert}. There are five Sub-Cases to be considered:

i) $0 < T^* < s/m$, the system (6) has two equilibria.
ii) $T^* = s/m$, here the system (6) has two equilibria.
iii) $s/m < T^* < \max T_{vert}(V) = T_{vert}(\widetilde{V}_1)$, the system (6) has three equilibria.
iv) $T^* = \max T_{vert}(V) = T_{vert}(\widetilde{V}_1)$, here the system (6) has two equilibria.
v) $T^* > \max T_{vert}(V) = T_{vert}(\widetilde{V}_1)$, the system (6) has one equilibrium point.

Before analyzing each possibility separately, let us write the Jacobian matrix of (6) for $k_1 \neq 1$. This is

$$J[f_1, f_2]_{(V,T)} = \begin{bmatrix} (N-k_2)T + g & (N-k_2)V \\ \dfrac{T - k_1 T(1+V)^2}{(1+V)^2} & -\dfrac{D(V)}{(1+V)} \end{bmatrix}, \tag{18}$$

where $D(V) = k_1 V^2 + rV + m$.

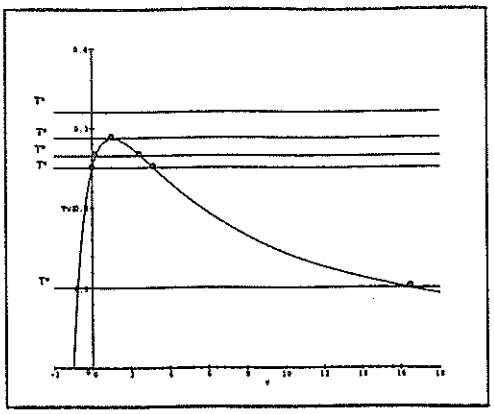

Fig. 7. Case **1.b:** This figure shows the relevant portion of the graph of T_v for $m + 1 - 2\sqrt{m} < k_1 < 1$ with $0 < m < 4$ and the different possibilities for T^*.

Case 1.b.i.

The system (6) has two equilibria: $Q = (0, s/m)$ and R. (Actually there are three, see Figure 8, but one of them is not in Ω, the region of biological interest.)

To obtain the local phase portrait around each equilibrium we evaluate (18) at Q, from which we determine

$$tr(J[f_1, f_2]_{(0,s/m)}) = \left[(N - k_2)\frac{s}{m} + g - m\right] < 0,$$

$$det(J[f_1, f_2]_{(0,s/m)}) = -m\left[(N - k_2)\frac{s}{m} + g\right] > 0.$$

Moreover, given that the eigenvalues, λ_1 and λ_2, of (18) are

$$\lambda_1 = \left[(N - k_2)\frac{s}{m} + g\right] < 0 \quad \text{and} \quad \lambda_2 = -m < 0,$$

then $Q = (0, s/m)$ is a locally asymptotically stable node. Now we obtain the abscissa of the points of intersection of the horizontal line $T^* = \frac{g}{(k_2 - N)}$ with the graph of the function T_{vert}. These are the roots of the quadratic polynomial

$$T^* k_1 V^2 + (rT^* - s)V + (T^* m - s) = 0,$$

i.e.,

$$V_1^*, V_2^* = \frac{-(rT^* - s) \pm \sqrt{(rT^* - s)^2 - 4T^* k_1 (T^* m - s)}}{2T^* k_1}. \tag{19}$$

Following from the condition $T^* < s/m$, we have $V_1^* > 0$ and $V_2^* < 0$ as shown in Figure 8.

Thus, we evaluate (18) at $R = (V_1^*, T^*)$ from which

$$tr(J[f_1, f_2]_{(V_1^* T^*)}) = -\frac{D(V_1^*)}{(1 + V_1^*)} < 0 \text{ and}$$

$$det(J[f_1, f_2]_{(V_1^*, T^*)}) = \frac{V_1^* g}{(1 + V_1^*)^2}[1 - k_1(1 + V_1^*)^2].$$

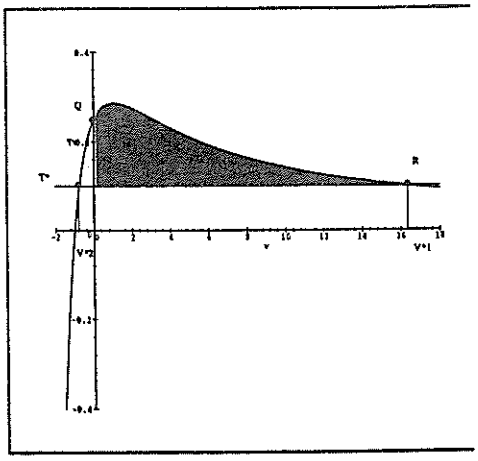

Fig. 8. Case **1.b.i:** Here the system (6) has three equilibrium points, but just two of them (Q and R) are biologically reasonable.

Because of the large number of parameters involved, it is not easy to determine the sign of $det\ J[f_1, f_2]_{(V_1^*, T^*)}$. In order to save work (particularly for the global analysis), the ideal approach then is the use the parameter values known in Table 1, to determine the sign of $det\ J[f_1, f_2]_{(V_1^*, T^*)}$. This would allow us to discriminate two behavior families: Saddle and non-saddle points.

Case 1.b.ii.

Here the system (6) has two equilibria: Q and R. Because of the condition $T^* = s/m$, V_1^* and V_2^* in (19) reduce to

$$V_1^* = 0 \quad \text{and} \quad V_2^* = -\frac{(rT^* - s)}{T^* k_1} = \left(\frac{1 - k_1}{k_1}\right) > 0.$$

Thus $Q = (0, s/m)$ and $R = (V_2^*, T^*)$. The graph of T_{vert} is sketched in Figure 9.

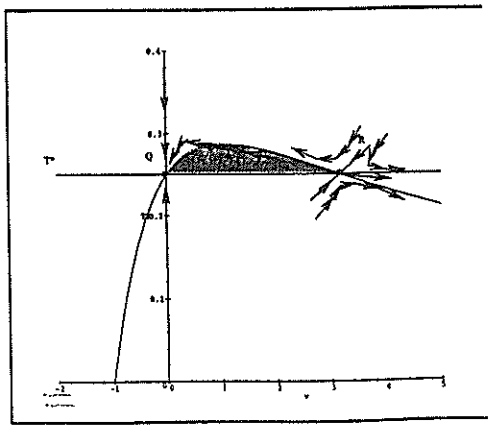

The positivity of V_2^* comes from the condition $m+1-2\sqrt{m} < k_1 < 1$. In order to get the local dynamics of (6) around each equilibria we evaluate the Jacobian at each.

At Q, (18) reduces to

$$J[f_1, f_2]_{(0,s/m)} = \begin{bmatrix} 0 & 0 \\ 0 & -m \end{bmatrix}. \tag{21}$$

Given that $tr\ J[f_1, f_2]_{(0,s/m)} = -m \neq 0$ and $det\ J[f_1, f_2]_{(0,s/m)} = 0$, Q is a non-hyperbolic point of co-dimension one. Moreover it is a saddle-node bifurcation point of (6). The eigenvalues are $\lambda_1 = 0$ and $\lambda_2 = -m$ and the corresponding eigenvectors are

$$\vec{v}_1 = \begin{bmatrix} 1 \\ \frac{s}{m^2}(1-k_1) \end{bmatrix} \quad \text{and} \quad \vec{v}_2 = \begin{bmatrix} 0 \\ 1 \end{bmatrix}.$$

Again, the Centre Manifold Theorem ensures us the existence of a positive invariant manifold of (6) containing the point Q and whose tangent vector at Q is $\vec{v}_1$. All the local dynamics of (6) around Q are given in terms of the dynamics around the center manifold.

Evaluating (18) at R, we obtain $det\ J[f_1, f_2]_{(V_2^*, T^*)} = \frac{s}{m}(k_1-1)^2(N-k_2) < 0$. Therefore R is a saddle point.

The eigenvalues are

$$\lambda_1, \lambda_2 = \frac{-\left[m + \left(\frac{1-k_1}{k_1}\right)m\right] \pm \sqrt{\left[m + \left(\frac{1-k_1}{k_1}\right)m\right]^2 - \frac{4s}{m}(k_1-1)^2(N-k_2)}}{2}$$

with $\lambda_1 > 0$ and $\lambda_2 < 0$. The associated eigenvectors are

$$\vec{v}_1 = (1+p_1^2)^{-1/2}\begin{bmatrix} 1 \\ p_1 \end{bmatrix} \quad \text{and} \quad \vec{v}_2 = (1+p_2^2)^{-1/2}\begin{bmatrix} 1 \\ p_2 \end{bmatrix},$$

where

$$p_1 = \frac{\lambda_1}{(N-k_2)\left(\frac{1-k_1}{k_1}\right)} < 0 \quad \text{and} \quad p_2 = \frac{\lambda_2}{(N-k_2)\left(\frac{1-k_1}{k_1}\right)} > 0.$$

Let us denote by $M(Q)$ the slope of the path of the center manifold of (6) at Q i.e.,

$$M(Q) = \frac{s}{m^2}(1-k_1) > 0.$$

Evaluating $T'_{vert}(V)$ at $V = 0$, we deduce $M(Q) = T'_{vert}(0)$.

We address the global analysis of the phase portrait of (6). The left unstable manifold, $W^u(R)$, of (6) at R leaves this point and enters the shaded region of Figure 9. Once there, the vector field pushes it up towards the graph of the nullcline T_{vert}, which it must cross with horizontal tangent vector. As time increases, $W^u(R)$ leaves the graph of T_{vert}, but again, the vector field pushes it down toward the center manifold of (6) ending at Q, as time goes to infinity.

The right unstable manifold of R runs away from R. Because of the vector field this tends to $(+\infty, 0)$ as t increases. This global behavior is shown in Figure 9. The analysis of this Case can be summarized in the following proposition.

Proposition 1.5. *If* $m+1-2\sqrt{m} < k_1 < 1$, $0 < m < 4$ *and* $T^* = \frac{g}{k_2 - N} = s/m$, *then the system (6) has: One non-hyperbolic point* (Q) *of co-dimension one and one hyperbolic saddle point* (R). *Moreover, the left unstable manifold of (6) at* R *reaches* Q *through the center manifold of (6) as* $t \to +\infty$ *and the right unstable manifold of (6) at* R *tends to* $(+\infty, 0)$ *as* $t \to +\infty$.

Case 1.b.iii.

Here we have

$$\frac{s}{m} < T^* < \frac{s}{2\sqrt{k_1} - k_1 + m - 1} \equiv \max T_{vert}(V)$$

with $m+1-2\sqrt{m} < k_1 < 1$ and $0 < m < 4$. In this Case, system (6) has three equilibria: $Q = (0, s/m)$, $R = (V_1^*, T^*)$ and $S = (V_2^*, T^*)$, where V_1^* and V_2^* are given by

$$V_1^*, V_2^* = \frac{-(rT^* - s) \pm \sqrt{(rT^* - s)^2 - 4T^* k_1 (T^* m - s)}}{2T^* k_1}. \tag{21}$$

Because of the previous conditions, $V_1^* > 0$ and $V_2^* > 0$ (See Figure 10).

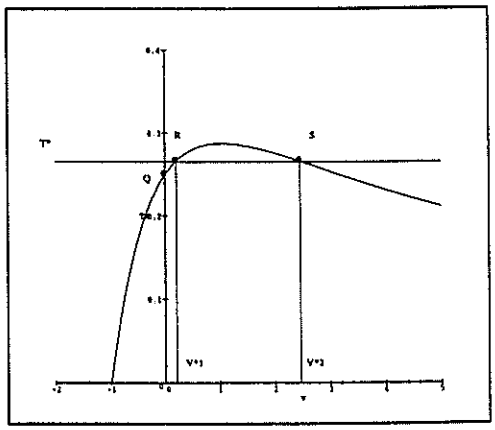

Fig. 10. Case **1.b.iii:** Here, $s/m < T^* < \max T_v(V)$.

The local phase portrait analysis follows as with previous arguments, and Q is a saddle node.

Continuing with our phase portrait analysis in a neighborhood of S, evaluating (18) at S yields the Jacobian from which it follows the

$$tr\ J[f_1, f_2]_{(V_2^*, T^*)} = -\frac{D(V_2^*)}{(1+V_2^*)} < 0 \text{ and}$$

$$det\ J[f_1, f_2]_{(V_2^*, T^*)} = \frac{V_2^* g}{(1+V_2^*)^2}[1 - k_1(1+V_2^*)^2].$$

Here the *det* has three cases for sign: $i) k_1(1+V_2^*)^2 - 1 > 0$, $ii) k_1(1+V_2^*)^2 - 1 = 0$ and $iii) k_1(1+V_2^*)^2 - 1 < 0$.

Using parameter values from Table 1, including conditions above, we find numerically that Case (iii) is the feasible Case, and hence S is a saddle node.

Case 1.b.iv.

Here we have

$$T^* = \frac{g}{k_2 - N} = T(\tilde{V}_1) = \frac{s}{2\sqrt{k_1} + m - k_1 - 1}$$

with $m + 1 - 2\sqrt{m} < k_1 < 1$ and $0 < m < 4$. Now the equilibria R and S of the previous possibility collapse into one equilibrium: E. It is easy to verify that for T^* as above, $V_1^* = V_2^* = \tilde{V} = \frac{1}{\sqrt{k_1}} - 1$. Thus, the pair of equilibria of (6) are given as follows $Q = (0, s/m)$ and $E = (\frac{1}{\sqrt{k_1}} - 1, T^*)$, as they are shown in the Figure 11(a).

Again, the local phase portrait analysis of (6) starts by evaluating the Jacobian matrix (18) at Q. This gives us

$$tr\ J[f_1, f_2]_{(0,s/m)} = (N - k_2)\frac{s}{m} + g - m \text{ and} \tag{22}$$

$$det\ J[f_1, f_2]_{(0,s/m)} = -m\left[(N - k_2)\frac{s}{m} + g\right]. \tag{23}$$

The condition $\frac{s}{m} < T^* = \frac{g}{k_2 - N}$ implies that $[(N - k_2)\frac{s}{m} + g] > 0$. Thus $det\ J[f_1, f_2]_{(0,s/m)} < 0$. Therefore Q is a saddle point. The eigenvectors of (23) are

$$\vec{v}_1 = \begin{bmatrix} \frac{[(N-k_2)\frac{s}{m}+g+m]}{(1-k_1)s/m} \\ 1 \end{bmatrix} \quad \text{and} \quad \vec{v}_2 = \begin{bmatrix} 0 \\ 1 \end{bmatrix}.$$

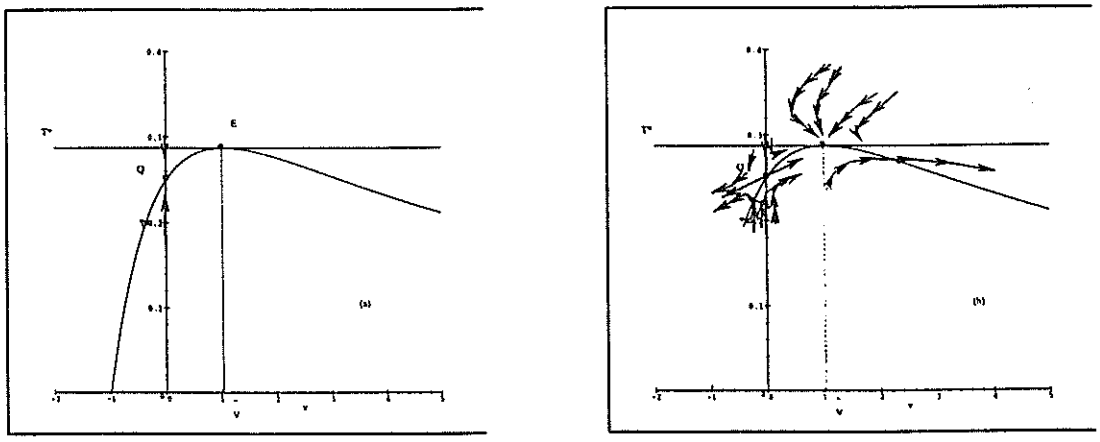

Fig. 11. Case **1.b.iv:** The situation for $T^* = \max T_{vert}(V)$. (a) The system (6) has two equilibria. (b) The local phase portrait of (6) around Q and E.

The stable manifold of (6) at Q has as tangent vector $\vec{v}_2$, while the unstable manifold locally has as tangent vector $\vec{v}_1$. See Figure 11(a).

Evaluating (18) at E we get the following

$$tr\ J[f_1, f_2]_{(\frac{1}{\sqrt{k_1}}-1, T^*)} = [k_1 + 1 - m - 2\sqrt{k_1}] < 0 \text{ and}$$
$$det\ J[f_1, f_2]_{(\frac{1}{\sqrt{k_1}}-1, T^*)} = 0.$$

Since the eigenvalues are $\lambda_1 = 0$ and $\lambda_2 = (k_1 + 1 - m - 2\sqrt{k_1})$, then the equilibrium E is a non-hyperbolic point of co-dimension one. The associated eigenvectors are

$$\vec{v}_1 = \begin{bmatrix} 1 \\ 0 \end{bmatrix} \quad \text{and} \quad \vec{v}_2 = \begin{bmatrix} \frac{(N-k_2)(\frac{1}{\sqrt{k_1}}-1)}{k_1+1-m-2\sqrt{k_1}} \\ 1 \end{bmatrix}.$$

More precise information on the local dynamics of the system (6) around the equilibrium can be obtained by using the Centre Manifold Theorem. For our purposes it is enough to say that E is a saddle-node bifurcation point. The local behavior of the trajectories of (6) can be seen in Figure 11(b).

In order to determine the global phase portrait of (6) in the region Ω, let us denote by $W^u(Q)$ the right unstable manifold of (6) at Q. Let $M^u(Q)$ be the slope of the path of $W^u(Q)$ at Q. To compare $M^u(Q)$ with $T'_{vert}(0)$, we examine the ratio: $\frac{M^u(Q)}{T'_{vert}(0)} = \frac{m}{(N-k_2)s/m+g+m}$. By using the condition $\frac{s}{m} < T^* = \frac{g}{k_2-N}$, hence it follows $M^u(Q) < T'_{vert}(0)$. The geometric interpretation of this inequality implies that the unstable manifold $W^u(Q)$ leaves the equilibrium Q below the graph of T_{vert} as it is shown in Figure 12(a).

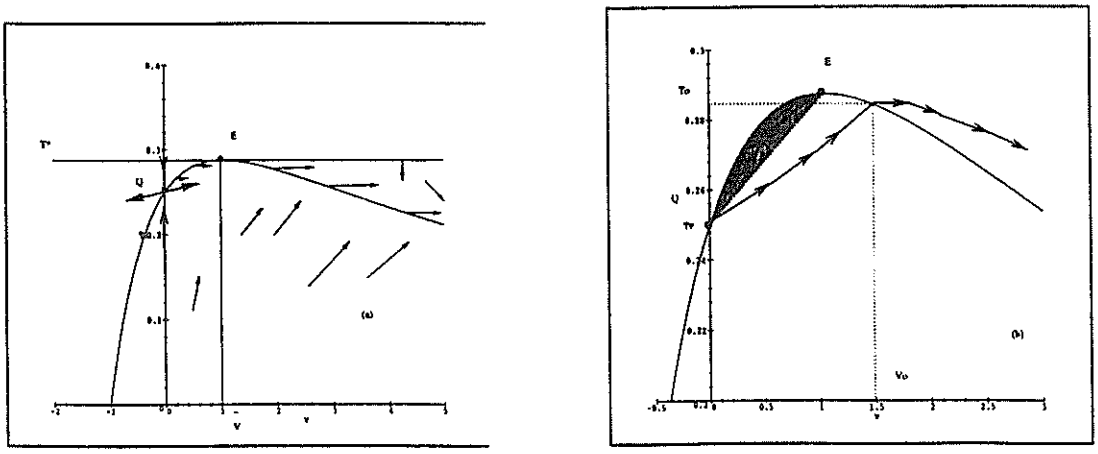

Fig. 12. Case **1.b.iv:** Behavior of the trajectories of $T^* = \max T_v$. (a) $W^u(Q)$ leaves Q in this way. (b) The two possible behaviors of $W^u(Q)$.

Once $W^u(Q)$ leaves Q, because of the vector field (6), $W^u(Q)$ initially will have two types of behavior as time t goes to infinity (Figure 12b):

i) $W^u(Q)$ ends at E. The unique way in which $W^u(Q)$ can reach E is through that part of the center manifold of (6) allocated in the nodal sector of E.

ii) $W^u(Q)$ tends to $(+\infty, 0)$. Once $W^u(Q)$ reaches the graph of T_{vert} (which must be at some point (V_0, T_0) with $V_0 > \widetilde{V}$ and $T_0 < T^*$) the vector field pushes it down in such a way that as the time increases $W^u(Q) \to (+\infty, 0)$.

In what follows, we will determine which set of parameters such that, in addition to satisfy the conditions of this Sub-Case, the above Cases could occur. For this, we consider the line which connects the points Q and E, i.e., that line whose equation is

$$T(V) = \left(\frac{T^* - s/m}{\widetilde{V}}\right) V + s/m, \tag{24}$$

with $0 \leq V \leq \widetilde{V}$. Let $\vec{n}_{\text{out}}$ be the normal vector of the above line pointing outward from the shaded region of Figure 12(b). Thus

$$\vec{n}_{\text{out}} = (T^* - s/m, -\widetilde{V}).$$

Now, we restrict the vector field (6) to the line (24). The resulting system is

$$\begin{aligned}
\dot{V} &= (NV - k_2 V)\left[\left(\frac{T^* - s/m}{\widetilde{V}}\right) V + s/m\right] + gV\ , \\
\dot{T} &= s - m\left[\left(\frac{T^* - s/m}{\widetilde{V}}\right) V + s/m\right] + \frac{V}{1+V}\left[\left(\frac{T^* - s/m}{\widetilde{V}}\right) V + s/m\right] \\
&\quad - k_1\left[\left(\frac{T^* - s/m}{\widetilde{V}}\right) V + s/m\right].
\end{aligned} \tag{25}$$

Given that on the graph of T_{vert} for $0 < V < \widetilde{V}$ the vector field points towards the shaded region of Figure 12(b), then for the set of parameters for which

$$[(\dot{V}, \dot{T}) \cdot \vec{n}_{\text{out}}] \leq 0 \qquad \forall\, V \in [0, \widetilde{V}], \tag{26}$$

where $(\dot{V}, \dot{T})$ is given in (25), we have proved that such a region is a positive invariant set of (6). Thus the unstable manifold $W^u(Q)$ ends at E as time t goes to infinity. Conversely, if for certain sets of parameters, we have

$$[(\dot{V}, \dot{T}) \cdot \vec{n}_{\text{out}}] > 0 \qquad \forall\, V \in (0, \widetilde{V}), \tag{27}$$

for $(\dot{V}, \dot{T})$ as in the system (25), then the shaded region of Figure 12(b) is not a positively invariant set of (6), resulting in $W^u(Q)$ crossing the graph of T_{vert} as shown in Case 1.b.ii. Now note that in that region of the first quadrant contained below the graphs of $T \equiv T^*$ and T_{vert}, both $\dot{V}$ and $\dot{T}$ are positive. In other words,

$$(\dot{V}, \dot{T}) \cdot \vec{n}_{\text{out}} = (T^* - s/m)\dot{V} - \widetilde{V}\dot{T}.$$

The inequality (26) implies

$$[(T^* - s/m)\dot{V}] \leq \widetilde{V}\dot{T}; \tag{28}$$

however, (27) yields:

$$[(T^* - s/m)\dot{V}] > \widetilde{V}\dot{T}. \tag{29}$$

To verify which situation is biologically feasible, we again turn to a numerical analysis using conditions of Case 1.b.iv and values from Table 1. We find that (29) holds true, and hence the shaded region is not a positively invariant of (6).

Case 1.b.v.

Here, $T^* > \max T_{vert}(V)$. In this Case, the system (6) has only one equilibrium: Q, which, according with previous analysis, is a hyperbolic saddle point. The right unstable manifold $W^u(Q)$ of (6) at Q crosses the graph of T_{vert} at the point (V_0, T_0) with $V_0 > \widetilde{V}$ and $T_0 < \max T_{vert}$. The vector field then pushes it down towards $(+\infty, 0)$ as time t goes to infinity (Figure 13).

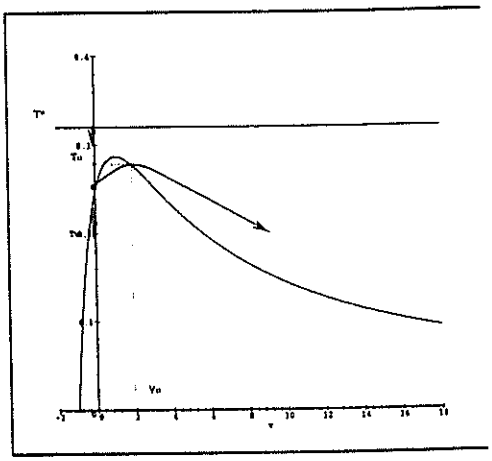

Fig. 13. Case **1.b.v:** This is the global phase portrait of (6) for $T^* > \max T_v(V)$.

Case 1.c.

Here $\widetilde{V}_1$ and $\widetilde{V}_2$ both are negative. The graph of T_{vert} is illustrated in Figure 14.

Again, depending on the value of T^* we have the following possibilities:

i) $0 < T^* < s/m$, the system (6) has two equilibria: R and Q. Note that there is a third equilibrium, but this not in the region of biological interest, hence, we leave it.
ii) $T^* = s/m$, the system (6) has just one equilibrium: Q.
iii) $T^* > s/m$, again here the system (6) has only one equilibrium.

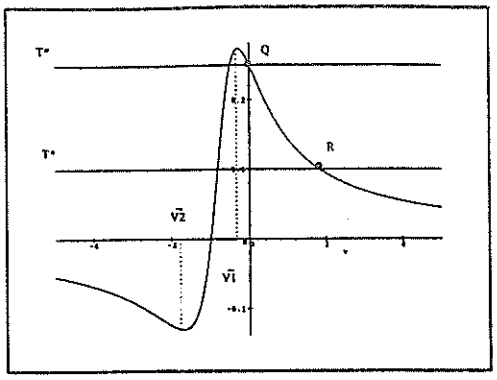

Fig. 14. Case **1.c:** This figure shows the graph of T_v for $1 < k_1 < m + 1 + 2\sqrt{m}$ with $0 < m < 4$ and the different possibilities for T^*.

Case 1.c.i.

Here, $1 < k_1 < m + 2\sqrt{m} + 1, 0 < m < 4$. The system (6) has two equilibria: $Q = (0, s/m)$ and $R = (V_1^*, T^*)$, where V_1^* is given in (21). For the local behavior of the trajectories of (6) we evaluate (18) at Q. By using some straightforward calculations one easily concludes that Q is a locally asymptotically stable node. The local analysis around R is not immediate. Numerically, we find it is a saddle node.

Case 1.c.ii.

System (6) has just one equilibrium $Q = (s/m, 0)$. The Jacobian matrix (18) at Q yields eigenvalues $\lambda_1 = 0$ and $\lambda_2 = -m$, with $det\ J[f_1, f_2]_{(s/m,0)} = 0$ and $tr\ J[f_1, f_2]_{(s/m,0)} = -m \neq 0$. The equilibrium Q is thus a saddle-node bifurcation point of (6). The corresponding eigenvectors are

$$\vec{v}_1 = \begin{bmatrix} \frac{1}{s(1-k_1)} \\ 1 \end{bmatrix} \quad \text{and} \quad \vec{v}_2 = \begin{bmatrix} 0 \\ 1 \end{bmatrix}.$$

Given the conditions on k_1 in this Sub-Case, we have $(1 - k_1) < 0$. Thus the trajectory of (6) which leaves Q through the center manifold of (6) tends to $(+\infty, 0)$ as time goes to infinity (Figure 15).

Case 1.c.iii: Q is a hyperbolic saddle point.

The right unstable manifold $W^u(Q)$ leaves Q and the vector field pushes it down towards $(+\infty, 0)$ where it ends as time t tends to $+\infty$.

This completes the main Case 1.

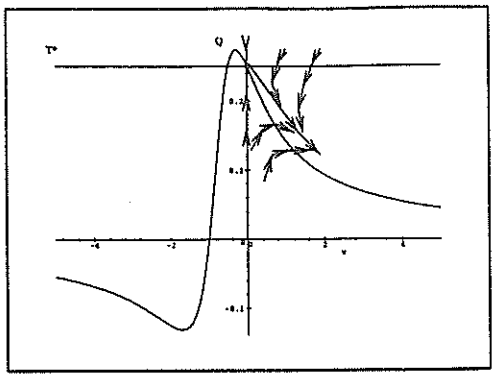

Fig. 15. Case **1.c.ii:** Global phase portrait of (6). See the text for details.

3.2. Phase Portrait Analysis in Case 2:

$$d = [(m - k_1)^2 - 2(m + k_1) + 1] = 0.$$

Here the denominator $D(V) = k_1V^2 + (k_1 + m - 1)V + m$ of the vertical nullcline (9) has just one real root V^*. In the mk_1-plane this occurs on the graph of the functions

$$k_1(m) = m + 1 - 2\sqrt{m} \quad \text{and} \quad k_2(m) = m + 1 + 2\sqrt{m}\ ,$$

as it is shown in Figure 1.

Again, the dynamics of (6) depend on both the profile of the vertical nullcline and the relative position of the horizontal null-cline (7) and (8). The first depends on which of the branches of the parabola in Figure 1 is under consideration. We analyze each Case separately.

Case 2.a: $k_1 = m + 1 - 2\sqrt{m}$.

Because of the condition $d = 0$, this implies that the root of D is

$$V^*(m) = \frac{\sqrt{m} - m}{m + 1 - 2\sqrt{m}}, \tag{30}$$

from which one can verify the following properties of V^*: i) $V^*(0) = 0$, ii) $V^* > 0 \Leftrightarrow m \in (0,1)$, iii) $V^* < 0 \Leftrightarrow m > 1$, iv) $V^* \to +\infty$ as $m \to 1^-$ and v) $V^* \to -\infty$ as $m \to 1^+$. The graph of V^* as a function of m, is shown in Figure 16.

Since D is a second order polynomial and V^* is its unique root, it can be written as $D(V) = A(V - V^*)^2$, where $A = \frac{m}{V^{*2}}$. Then the vertical nullcline (7) takes the form

$$T_{vert}(V) = \frac{V^{*2}}{m}\frac{(s + sV)}{(V - V^*)^2}. \tag{31}$$

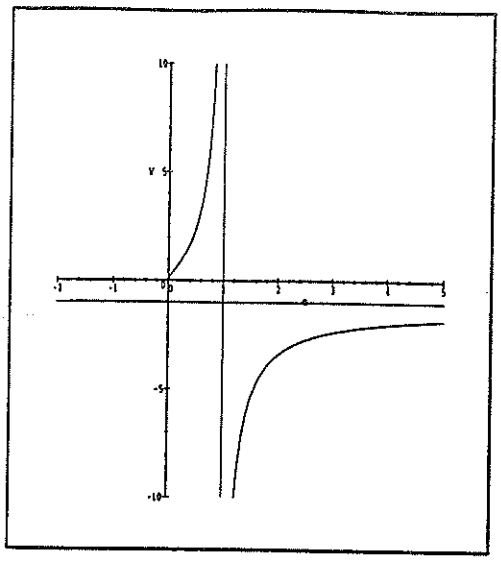

Fig. 16. Case **2.a:** Behavior of V^* as a function of m.

The graph of this function is sketched in Figure 17 for different parameter ranges. If we compare the qualitative behavior of the graphs in Figures 17(a)-(c) on the region Ω, one can see that the above profiles of T_{vert} coincide with those given in Figures 14, 2 and 7, respectively. Thus, for dynamical purposes of the system (6), the behavior is essentially the same.

Figure 17(d) is the new Case. Thus, we will focus on analyzing the phase portrait of (6) for each one of the possibilities illustrated in Figure 18. To do this, we first compute the abscissas of the intersections of T^* with the graph of T_{vert}. Thus, we seek the values of V such that

$$T_{vert}(V) = T^* \Leftrightarrow \frac{V^{*2}}{m}\frac{(s+sV)}{(V-V^*)^2} = T^* = \frac{g}{(k_2-N)}.$$

These are roots of the quadratic polynomial

$$mT^*V^2 - (2V^*mT^* + sV^{*2})V + mV^{*2}T^* - V^{*2}s = 0, \tag{32}$$

or

$$V_1^*, V_2^* = \frac{(2V^*mT^* + sV^{*2}) \pm V^*\sqrt{4V^*smT^* + s^2V^{*2} + 4mT^*s}}{2mT^*}, \tag{33}$$

where V^* is given by the equality (30), with $m \in (0,1)$. Now we begin the phase portrait analysis for each of the three Cases depicted in Figure 18.

Case 2.a.i: $0 < T^* < s/m$.

In the region of biological interest Ω, the system (6) has two equilibria: $Q = (0, s/m)$ and $R = (V_1^*, T^*)$, where V_1^* is the positive root of (32) (Figure 18). A similar analysis can be used in this case to verify Figure 19 is indeed the behavior of the phase portrait. The following proposition summarizes that analysis.

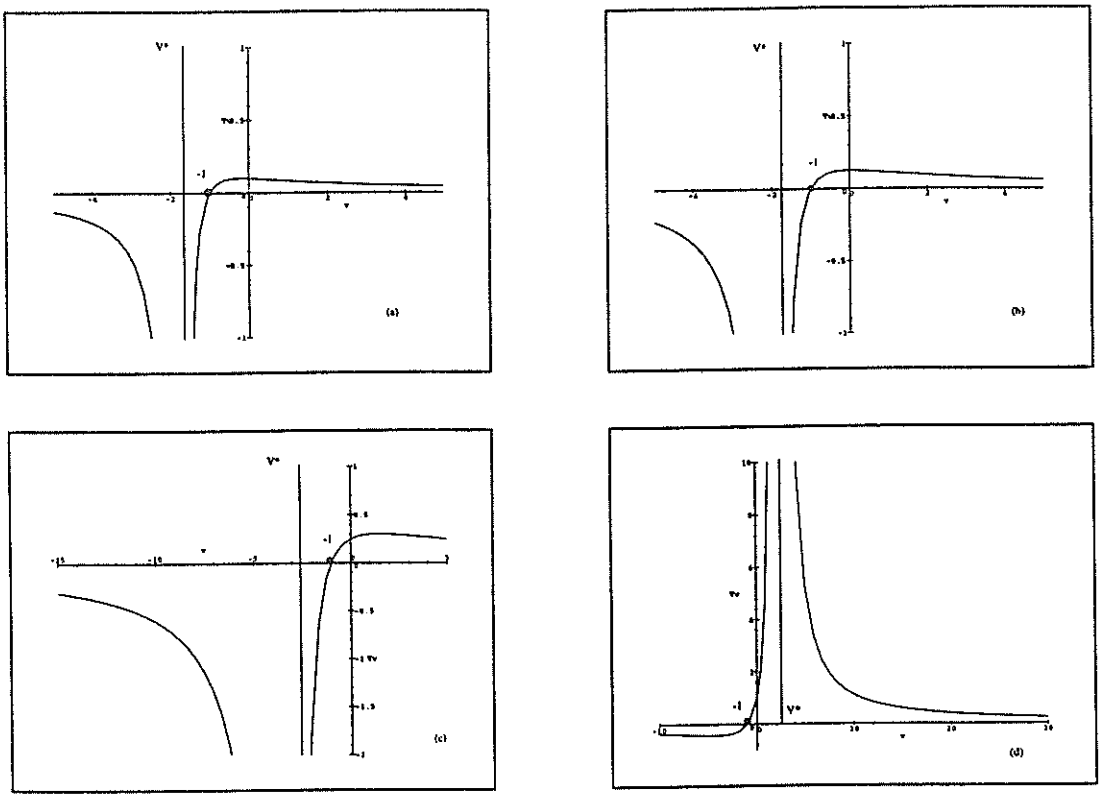

Fig. 17. Case **2.a:** Behavior of T_{vert} for different values of m (i.e of $k_1 = m + 1 - 2\sqrt{m}$) (a) for $m > 4$ (i.e. for $k_1 > 1$). (b) $m = 4$ and $k_1 = 1$. (c) For $m \in (1, 4)$ (i.e. $0 < k_1 < 1$). (d) For $m \in (0, 1)$.

Proposition 2.1. *If $k_1 = m + 1 - 2\sqrt{m}$ with $m \in (0, 1)$, then for each T^* such that $T^* = g/(k_2 - N) < s/m$, the system (6) has two equilibria: One locally asymptotically stable node (Q) and a saddle point (R). Moreover, the left unstable manifold $W^u(R)$ of (6) at R ends at Q as $t \to +\infty$, i.e., $W^u(R)$ is a saddle (R)-node (Q) heteroclinic trajectory of (6).*

Case 2.a.ii: $T^* = s/m$.

From the equality (33), we have $V_1^* = V^*(2 + V^*)$ and $V_2^* = 0$. Here, the system (6) has two equilibria: $Q = (0, s/m)$ and $R = (V^*(2 + V^*), s/m)$. As in the Case 2.a.1, we can prove the behavior shown in Figure 20. The result is summarized in the following proposition.

Proposition 2.2. *If $k_1 = m + 1 - 2\sqrt{m}$ with $m \in (0, 1)$, then for each $T^* = g/(k_2 - N) = s/m$, the system (6) has two equilibria: A saddle-node bifurcation point (Q) and a hyperbolic saddle point. Moreover, the left unstable manifold of Q connects the equilibria R and Q.*

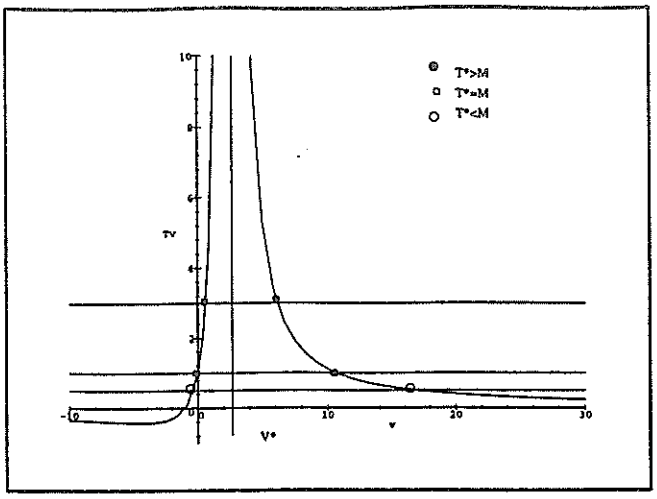

Fig. 18. Case **2.a:** This figure shows the graph of T_v for $k_1 = m+1-2\sqrt{m}$ with $m \in (0,1)$ and the different possibilities for T^*.

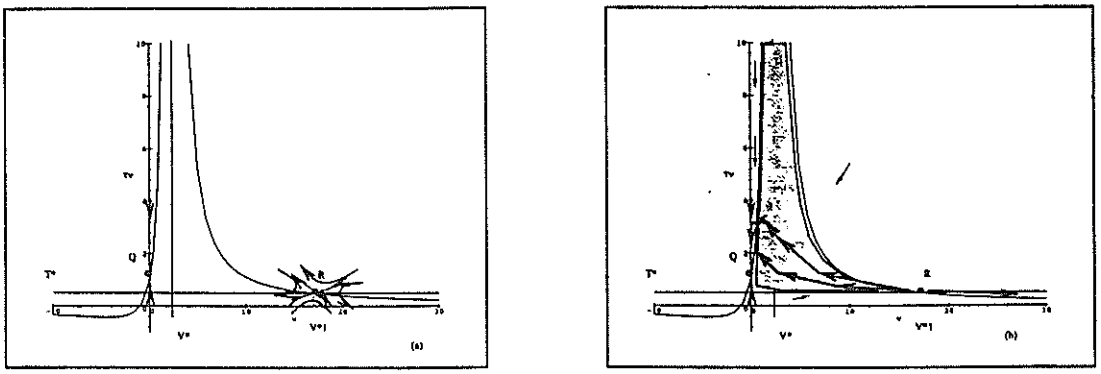

Fig. 19. Case **2.a.i:** Dynamics of (6) for $k_1 = m + 1 - 2\sqrt{m}$ with $0 < T^* < M$. (a) Local phase portrait. (b) Global phase portrait.

Case 2.a.iii.

Figure 18 shows the three equilibrium points of system (6) in Ω: $Q = (0, s/m)$, $R = (V_1^*, T^*)$ and $S = (V_2^*, T^*)$, where V_1^* and V_2^* are given in (33) with V_1^* and V_2^* both positive and $V_1^* > V_2^*$.

The Jacobian matrix at Q is written as follows

$$J[f_1, f_2]_{(0,s/m)} = \begin{bmatrix} (N-k_2)\frac{s}{m} + g & 0 \\ -s + \frac{2s}{\sqrt{m}} & -m \end{bmatrix}, \quad \text{such that}$$

$$tr\ J[f_1, f_2]_{(s/m,0)} = \left[(N-k_2)\frac{s}{m} + g - m\right] \text{ and}$$

$$det\ J[f_1, f_2]_{(s/m,0)} = -m\left[(N-k_2)\frac{s}{m} + g\right].$$

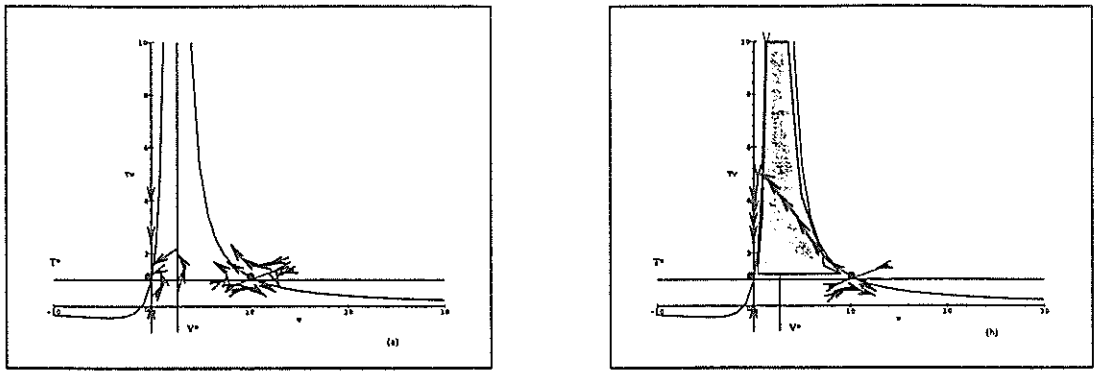

Fig. 20. Case **2.a.ii:** Dynamics of the system (6) for (a) Local behavior of the trajectories (b) Global dynamics in the region of biological interest.

The inequality $\frac{g}{(k_2-N)} > \frac{s}{m}$ implies $det\ J[f_1, f_2]_{(s/m,0)} < 0$, therefore Q is a hyperbolic saddle point. The eigenvalues are $\lambda_1 = \left[(N-k_2)\frac{s}{m} + g\right] > 0$ and $\lambda_2 = -m < 0$. The corresponding eigenvectors are

$$\vec{v}_1 = \begin{bmatrix} \frac{(N-k_2)\frac{s}{m}+g+m}{-s+\frac{2s}{\sqrt{m}}} \\ 1 \end{bmatrix} \quad \text{and} \quad \vec{v}_2 = \begin{bmatrix} 0 \\ 1 \end{bmatrix}.$$

The analysis of R and S are similar to Case 1.b.ii. Thus R is a saddle and S is a locally asymptotically stable node. This is also verified numerically.

Case 2.b: $k_1 = m + 1 + 2\sqrt{m}$.

Here the real root of D can be written as follows

$$V^* = -\frac{\sqrt{m}+m}{m+1+2\sqrt{m}} < 0, \qquad \forall\ m > 0,$$

and $V^* = 0$ for $m = 0$. From the above expression for V^* is straightforward to conclude that $-1 < V^* \leq 0$. Thus, the graph of the vertical nullcline is as in Figure 21.

If we observe Figure 21(a) we note that the tail of the graph of T_{vert} in the region Ω has the same features as that part of the graph of T_{vert} in the same region in Figure 14. For this reason the results given in Case 1.c.i and ii hold here.

In Figure 21(b) we have an extreme situation whose main feature is that the equilibrium of (6) which comes from the intersection of the graph of T_{vert} with the vertical axis runs away to $(0, +\infty)$. Thus, for finite values of the variables V and T, whatever the value of T^* is, the system (6) has just one equilibrium.

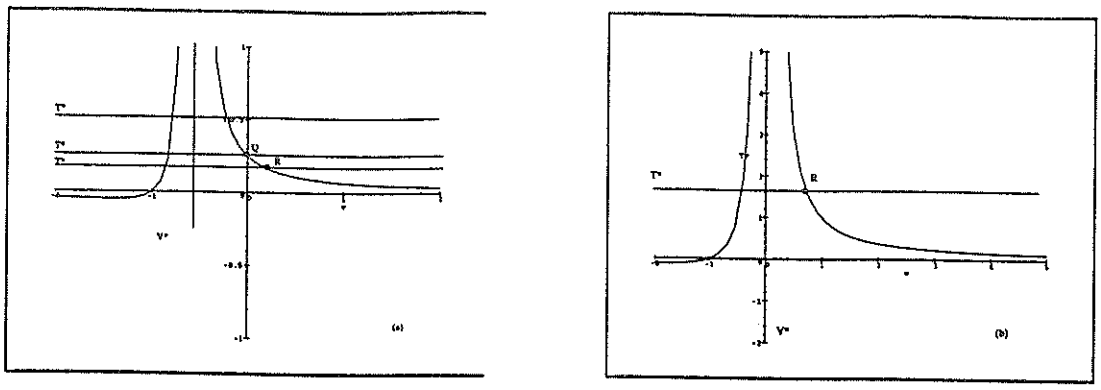

Fig. 21. Case **2.b:** Qualitative behavior of T_v for $k_1 = m + 1 + 2\sqrt{m}$ and for different values of m. (a) $m > 0$. (b) $m = 0$.

3.3 Phase Portrait Analysis in Case 3:

$$d = [(m - k_1)^2 - 2(m + k_1) + 1] > 0.$$

Here the denominator $D(V) = k_1V^2 + (k_1 + m - 1)V + m$ has two real roots, V_1 and V_2. Hence D can be written as $D(V) = A(V - V_1)(V - V_2)$, where $A = m/V_1V_2$. The vertical nullcline takes the form

$$T_{vert}(V) = \frac{V_1V_2s(1 + V)}{(V - V_1)(V - V_2)}.$$

For $k_1 > 0$ and $m > 0$, neither V_1 or V_2 is zero. Depending on the sign of $(m + k_1 - 1)$ we have different Cases.

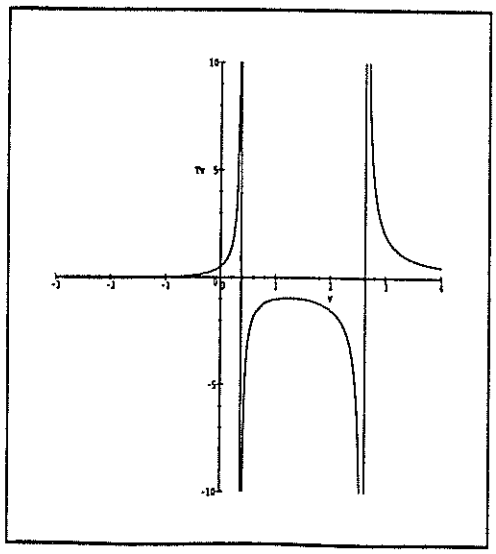

Fig. 22. Case **3.a:** The qualitative behavior of T_v.

Case 3.a.

If $(m + k_1 - 1) < 0$, both V_1 and V_2 are positive. The qualitative behavior of T_{vert} is shown in Figure 22.

Again, depending on $T^* = \frac{g}{k_2 - N}$, we have three Sub-Cases:

Sub-Case 3.a.i: $0 < T* < s/m$.

Here system (6) has two equilibria in the region Ω: $Q = (0, s/m)$, and $R = (V_1^*, T^*)$, where V_1^* is given by the equality (19). By using the linear approximation of (6) around Q one conclude that this equilibrium is an asymptotically stable node.

Although the local phase portrait analysis of (6) around R must be analyzed, our numerical simulations suggest that R is a hyperbolic saddle point. The local phase portrait is shown in Figure 23(a).

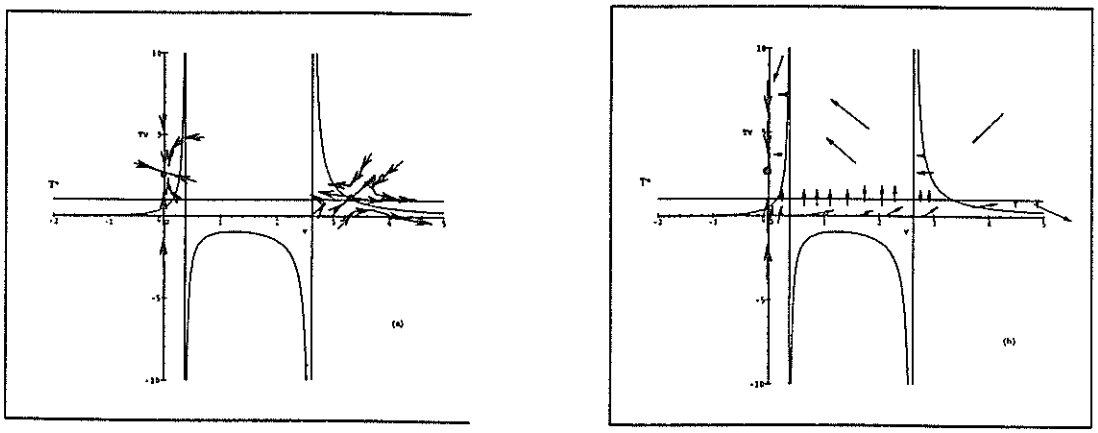

Fig. 23. Case **3.a.i:** The local phase portrait of (6) around Q and R (a). The direction field plot for (6) (b).

For the global analysis we note that the vector field defined by (6) is shown in Figure 23 (b). Hence, once the left unstable manifold, $W^u(R)$ leaves R the vector field pushes it up towards the equilibrium Q where it ends as $t \to +\infty$. The left stable manifold, $W^s(R)$, of R comes from some point on the vertical and reaches R for $t + \infty$. In Figure 24 we have done a numerical simulation to illustrate this.

Sub-Case 3.a.ii: $T^* = s/m$.

Here the system (6) has two equilibria in the region Ω: $Q = (0, s/m)$ and $R = (V_1^*, s/m)$.

The linear analysis of (6) around Q implies that this point is a nonhyperbolic equilibrium of saddle-node type and R is a saddle hyperbolic point. The global analysis follows the same reasoning as that given in the previous Sub-Case. Thus one conclude that $W^u(R)$ tends to Q as t increases. The way in which $W^u(R)$ approaches Q is as is illustrated in Figure 25.

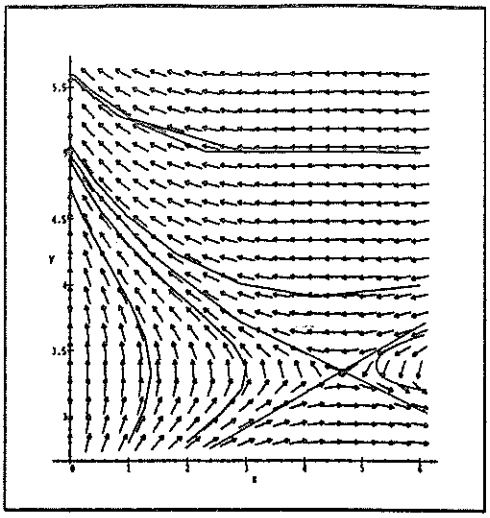

Fig. 24. Case **3.a.i:** Numerical simulations.

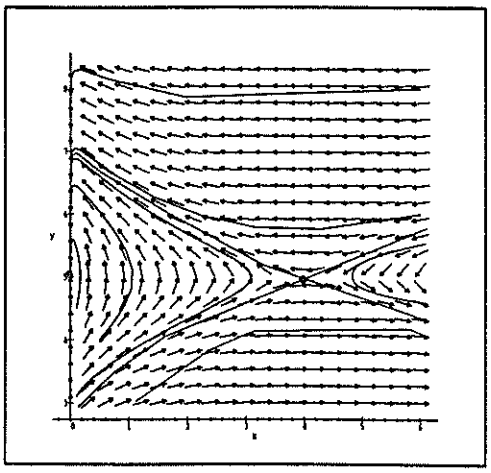

Fig. 25. Case **3.a.ii:** Numerical simulations.

Sub-Case 3a.iii.: $T^* > s/m$.

Here, in addition to $Q = (0, s/m)$ and $R = (V_1^*, T^*)$, a third equilibrium point $S = (V_2^*, T^*)$ of (6), emerges.

The local analysis of (6) around Q tells us that this equilibrium is a saddle node. The numerical phase portrait lends insights on the dynamics associated with the system in the region Ω. In particular note the damped oscillatory behavior of the trajectories of (6) around the equilibrium S, which leads to the left unstable manifold, $W^u(R)$, tending to S as t goes to infinity as is shown in Figure 26.

In Figure 27 we can see a closer picture of the phase portrait of (6) around S and the oscillations are illustrated.

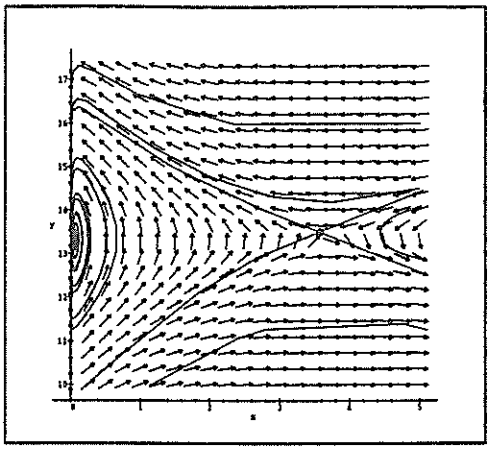

Fig. 26. Case **3.a.iii:** Numerical simulations.

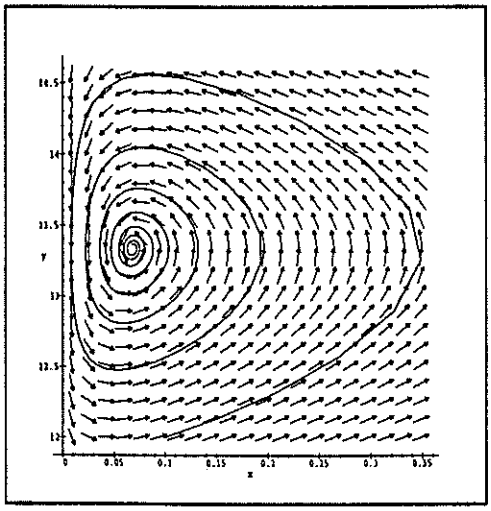

Fig. 27. Case **3.a.iii:** Numerical simulations close-up.

Case 3.b.

If $(m + k_1 - 1) = 0$, the roots V_1^* and V_2^* of the denominator D have opposite signs. The qualitative behavior of the vertical nullcline is as is shown in Figure 28.

Case 3.c.

If $(m+k_1-1) > 0$, both V_1^* and V_2^* are negative, hence the vertical asymptotes of the function D are shown in Figure 29.

Given that in the region of biological interest we have the same qualitative behavior as that in the Sub-Case 2.b which, in turn, corresponds to that in Figure 14; thus, we avoid the detailed analysis here of these two Cases.

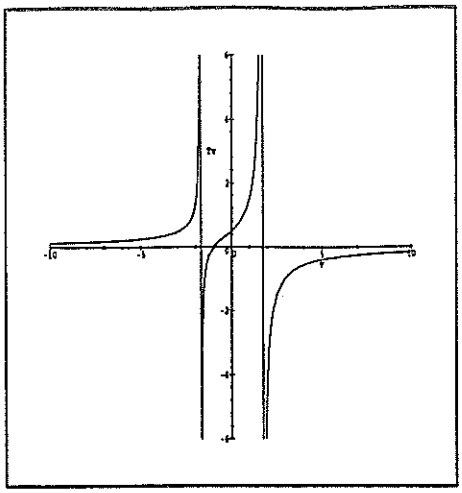

Fig. 28. Case **3.b:** The qualitative behavior of the vertical null-cline.

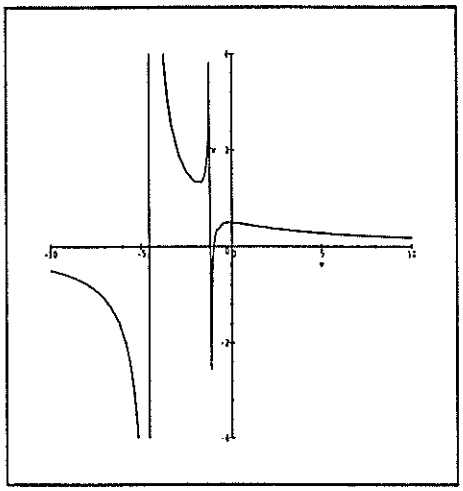

Fig. 29. Case **3.c:** The qualitative behavior of the vertical null-cline.

§4. Discussion

We have presented a very simple model of HIV and the immune system. The model accounts for many of the key dynamical behavior seen in the clinical investigations of HIV infection. In particular, the possibility of multiple steady states which are feasible by this model can allow for a wide range of clinical outcomes. In examining these steady states, we can directly tie the mathematical results to the observed biological phenomena, as follows.

The fixed point $Q = (0, \bar{T})$ represents an uninfected individual. We first want the model to make biological sense in the absence of HIV. This steady state accounts for this, i.e. and *uninfected steady state.* Secondly, the model should encompass the possible scenario that HIV can be cleared after introduction into a host. This may happen due to a low initial innoculum, in

which case HIV may get cleared by a natural immune response. Or, whether by drug therapy or enhanced immune environment, the potential for clearance should be possible. There are a few documented cases of this which are mostly pediatric infections, since vertical transmission can be monitored. However, since most initial infection in adults are not traceable to the moment of HIV transferral, (except maybe via blood transfusions), these data are difficult to gather.

This steady state would be expected to be stable up to a certain point (this point could be based on a number of individual features) at which time it would loose stability to one of the infected steady states.

There are two main non-zero steady states (referred to as R and S). These are the *infected steady states.* What is of key interest here is that both of these steady states have the same ordinate i.e. in that the horizontal nullcline T^* (which is a straight line) crosses the vertical nullcline (which is parabolic shaped in that region) twice. Hence, for a given value of the T steady state, there are two possibilities for the viral load value. We distinguish $R = (V_1, \bar{T})$ and $S = (V_2, \bar{T})$ by the fact that $V_2 > V_1$.

In the analysis, every case points to R as an unstable node, and S as a stable node. The idea then is as follows. When only R is present with Q, Q is the stable steady state and R is unstable. This would imply that a small viral load can be cleared. When both infected steady states are present, namely R and S, then Q and R are unstable and S is the stable node. The question then arises, why would the infected steady state with the higher viral load be the stable one? There is now clinical evidence to suggest that the viral loads are very high during latency Ho et al. [2], Wei et al. [16]. There is a high turnover rate for both T cells and virus during the period which traditionally was viewed as a "latent" period. In actuality, there is much taking place during this time. Hence, a higher viral load would make sense in this long infected steady state. We also know there is much antigenic variation within HIV within a given individual. Many strains may comprise the total V population, and since they may be in competition, this may drive the viral population to higher levels. These ideas may explain how the heteroclinic orbit leaving R and going to S is achieved.

Finally, there is a third outcome for the model which was only indirectly addressed in the steady state analysis. It is the *Progression to AIDS state.* This is characterized by the collapse of the $CD4^+$ T cell populations, and the large numbers of virus. Although this is not a steady state, it is a behavior of this system. When all the steady states become unstable, then it is this "state" which is the "stable" one; and hence all the trajectories are drawn to $(V = \infty, T = 0)$.

It should be noted here that in the dynamics of HIV and other diseases, such as cancer, disease progression states are not states of stabilization, but states where there is a rapid physical collapse of the system. In these models, the infected steady state (latency period) is a state of stabilization; however the progression to AIDS is not, since the viral population will eventually, in all infection cases, grow without bound.

TABLE 1
Variables and Parameters

Dependent Variables		Values
$T(t)$	= $CD4^+$ T cell population	1000 mm^{-3}
$V(t)$	= Infectious virus population (HIV)	$1.0 \times 10^{-3} mm^{-3}$
Parameters and Constants		**Values**
σ	= source of new $CD4^+$T cells	10 $d^{-}1$
μ	= death rate of $CD4^+$ T cell population	0.02 d^{-1}
$K_{V,T}$	= rate $CD4^+$ T cells becomes infected by free virus	2.4×10^{-5} mm^3 d^{-1}
$K_{T,V}$	= rate HIV is cleared	7.4×10^{-4} mm^3 d^{-1}
p	= maximal proliferation of the $CD4^+$ T cells	0.01 d^{-1}
$\hat{N}$	= production # of virus	10
C	= half saturation constant of the proliferation process	100 mm^{-3}
G_V	= growth rate of external viral source	2 d^{-1}
T_{max}	= Maximal population of T cells	1500 mm^{-3}
s	$= \frac{\sigma}{T_{max} \cdot p}$	
m	$= \frac{\mu}{p}$	
k_1	$= \frac{K_{V,T} K}{p}$	
N	$= \frac{\hat{N} K_{V,T} T_{max}}{p}$	
k_2	$= \frac{K_{T,V} T_{max}}{p}$	
g	$= \frac{G_V}{p}$	

TABLE 2.A
Phase Portrait Analysis in Case 1

CASE I:

Restriction: $d = [(m-k_1)^2 - 2(m+k_1)+1] < 0$ where d is the discriminant of the roots of the denominator of T_{vert}.

The following are defined for this case: $T_{vert} = \frac{s+sv}{k_1V^2+rV+m}$, $\max T_{vert} = \frac{s}{2\sqrt{k_1}-k_1+m-1}$, for Case I.a,

$\max T_{vert} = \frac{s}{m} = M$, and $T_{hor} = T^* = \frac{g}{k_2-N}$

SUB-CASE	SUB-SUB CASE	Steady States (S.S.)	Stability of S.S.	Figure Refrences
Ia. $m+1-2\sqrt{m} < k_1 < m+1+2\sqrt{m}$ $k_1 = 1$ and $0 < m < 4$				Fig. 1
	Iai. $0 < T^* < M$	1. $Q = (0, \frac{s}{m})$ 2.$R = (V^*, \frac{g}{k_2-N})$ 3. P = negative root	1. locally asymptotically stable node 2. hyperbolic saddle point 3. biologically infeasible, therefore not important	Figs. 2-4
	Iaii. $T^* = M$	1. $Q = (0, \frac{s}{m})$	1. saddle-node bifurcation point	Fig. 5
	Iaiii. $T^* > M$	1. $Q = (0, \frac{s}{m})$	1. saddle-node bifurcation point	Fig. 6
Ib. $m+1-2\sqrt{m} < k_1 < 1$ $0 < m < 4$				Fig. 7
	Ibi. $0 < T^* < M$	1. $Q = (0, \frac{s}{m})$ 2.$R = (V_1^*, T^*)$	1.locally asymptotically stable node 2. saddle node	Fig. 8
	Ibii. $T^* = M$	1. $Q = (0, \frac{s}{m})$ 2.$R = (V_1^*, T^*)$	1.non-hyperbolic point of co-dimension one 2. saddle node	Fig. 9
	Ibiii. $M < T^* < \max T_{vert}$	1. $Q = (0, \frac{s}{m})$ 2.$R = (V_1^*, T^*)$ 3.$S = (V_2^*, T^*)$	1. saddle point node 2. saddle point node 3. locally asymptotically stable node	Fig. 10
	Ibiv. $T^* = maxT_{vert}$	1. $Q = (0, \frac{s}{m})$ 2.$E = (\frac{1}{\sqrt{k_1}}, T^*)$	1. saddle point node 2. saddle-node bifurcation point	Figs. 11,12
	Ibv. $T^* > maxT_{vert}$	1. $Q = (0, \frac{s}{m})$	1. saddle point node	Fig. 13
Ic. $1 < k_1 < m+2\sqrt{m}+1$ $0 < m < 4$				Fig. 14
	Ici. $0 < T^* < M$	1. $Q = (0, \frac{s}{m})$ 2. $R = (V_1^*, T^*)$	1. locally asymptotically stable node 2. saddle node	
	Icii. $T^* = M$	1. $Q = (0, \frac{s}{m})$	1. saddle-node bifurcation	Fig. 15
	Iciii. $T^* > M$	1. $Q = (0, \frac{s}{m})$	1. hyperbolic saddle point	

TABLE 2.B
Phase Portrait Analysis in Case 2
Restrictions: $d = [(m-k_1)^2 - 2(m+k_1)+1)] = 0$.

$$\max T_{vert} = \frac{V^{*2}(s+sv)}{m(V-V^*)^2}$$

$$T^* = \frac{g}{k_2 - N}$$

$$M = \frac{s}{m}$$

$$V^* = \frac{\sqrt{m}-m}{m+1-2\sqrt{m}} \text{ for Case II.a}$$

$$V^* = -\frac{\sqrt{m}+m}{m+1+2\sqrt{m}} < 0 \; \forall \; m > 0 \text{ for Case II.b.}$$

SUB-CASE	SUB-SUB CASE	Steady States (S.S.)	Stability of S.S.	Figure References
IIa. $k_1 = m+1-2\sqrt{m}$ $V^*(0) = 0$ $V^* > 0 \Leftrightarrow m \in (0,1)$ $V^* < 0 \Leftrightarrow m > 1$ $V^* \to +\infty$ as $m \to 1^-$ $V^* \to -\infty$ as $m \to 1^+$				Figs. 16,17 There are 4 graphs drawn and a-c show the same type of behavior as previously analyzed, hence, they will be ignored and we'll focus on the d
	IIai. $0 < T^* < M$	1. $Q = (0, \frac{s}{m})$ 2. $R = (V_1^*, T^*)$	1. locally asymptotically stable node 2. hyperbolic saddle pt.	Figs. 18,19
	IIaii. $T^* = M$	1. $Q = (0, \frac{s}{m})$ 2. $R = (V^*(2+V^*), \frac{s}{m})$	1. saddle-node bifurcation point 2. hyperbolic saddle pt.	Figs. 18,20
	IIaiii. $T^* > M$	1. $Q = (0, \frac{s}{m})$ 2. $R = (V_1^*, T^*)$ 3. $S = (V_2^*, T^*)$	1. hyperbolic saddle pt. 2. saddle node 3. locally asymptotically stable node	Fig. 18
IIb. $k_1 = m+1+2\sqrt{m}$				Fig. 21
	IIbi. $m > 0$ $0 < T^* < M$	1. $Q = (0, \frac{s}{m})$ 2. $R = (V_1^*, T^*)$	1. locally asymptotically stable node 2. saddle point	Fig. 21a
	IIbii. $m > 0$ $T^* = M$	1. $Q = (0, \frac{s}{m})$	1. saddle point	Fig. 21a
	IIbiii $m > 0$ $T^* > M$	1. $Q = (0, \frac{s}{m})$	saddle point	Fig. 21a
	IIbiv $m = 0$	1. $R = (V_1^*, T^*)$	1. saddle point	Fig. 21b

TABLE 2.C
Phase Portrait Analysis in Case 3
Restrictions: $d = |(m-k_1)^2 - 2(m+k_1)+1| > 0$

SUB-CASE	SUB-SUB CASE	Steady States (S.S.)	Stability of S.S.	Figure References
III.a. $m+k_1-1<0$				Fig. 22
	III.a.i $0<T^*<\frac{s}{m}$	1. $Q=(0,\frac{s}{m})$ 2. $R=(V_1^*,T^*)$	1. asymptotically stable node 2. hyperbolic saddle point	Figs. 23,24
	III.a.ii $T^*=\frac{s}{m}$	1. $Q=(0,\frac{s}{m})$ 2. $R=(V_1^*,\frac{s}{m})$	1. Non-hyperbolic saddle node 2. hyperbolic saddle point	Fig. 25
	III.a.iii $T^*>\frac{s}{m}$	1. $Q=(0,\frac{s}{m})$ 2. $R=(V_1^*,T^*)$ 3. $S=(V_2^*,T^*)$	1. saddle node 2. saddle node 3. locally asymptotically stable node	Figs. 26,27
III.b. $m+k_1-1=0$				Fig. 28
III.c. $m+k_1-1>0$				Fig. 29

Acknowledgments. Part of this work was supported under grant number DMS 9596073 from the National Science Foundation. Part of this paper was carried out during FSG's sabbatical at the Centre for Mathematical Biology at Oxford. He thanks them for the hospitality during his stay. Also he wishes to thank the CONACYT-Mexico and the Facultad de Ciencias-UNAM for their support during this research.

References

1. J. Carr, *Applications of Centre Manifold Theory*, Springer-Verlag, New York, Heidelberg, Berlin, 1981.
2. D. D. Ho et al., Rapid turnover of plasma virions and CD4 lymphocytes in HIV-1 infection, Nature **373** (1995), 123–126.
3. D. W. Jordan and P. Smith, *Nonlinear Ordinary Differential Equations*, Clarendon Press, Oxford, 1994.
4. D. Kirschner and G. F. Webb, A model for treatment strategy in the chemotherapy of AIDS, Bulletin of Mathematical Biology **58**(2) (1996), 367–390.
5. D. Kirschner and G. F. Webb, Qualitative differences in HIV chemotherapy between resistance and remission outcomes, Emerging Infectious Diseases **3**(3) (1997), 273–283.
6. D. Kirschner and G. F. Webb, Understanding drug resistance in the monotherapy treatment of HIV infection, Bulletin of Mathematical Biology **59**(4) (1997), 763–785.

7. D. Kirschner and G. F. Webb, A mathematical model of combined drug therapy of HIV infection, Journal of Theoretical Medicine 1 (1997), 25–34.
8. D. Kirschner and G. F. Webb, Immunotherapy of HIV-1 infection, Journal of Biological Systems, to appear (1998).
9. A. Lafeuillade, C. Poggi, N. Profizi et al., Human immunodeficiency virus type 1 in lymph nodes compared with plasma, J. Infec. Diseases, **174** (1996), 404–407.
10. R. M. May and R. M. Anderson, Transmission dynamics of HIV infection, Nature **326** (1987), 137–42.
11. A. McLean and M. Nowak, Competition between AZT sensitive and AZT resistant strains of HIV, AIDS **6** (1992), 71–79.
12. A. R. McLean and M. A. Nowak, Interactions between HIV and other pathogens, J. Theoret. Biol. **155** (1991), 69–86.
13. M. A. Nowak and R. M. May, AIDS pathogenesis: Mathematical models of HIV and SIV infections, AIDS **7**(supp) (1993), 3–s18.
14. A. Perelson et al., HIV-1 Dynamics in vivo: Clearance rate, infected cell lifespan, and viral generation time, Science **271** (1996), 1582–1586.
15. A. Perelson, D. Kirschner and R. De Boer, The dynamics of HIV infection of $CD4^+$ T cells, Math. Biosciences **114** (1993), 81–125.
16. X. Wei et al., Viral dynamics in human immunodeficiency virus type 1 infection, Nature **373** (1995), 117–122.

Faustino Sánchez Garduño
Departamento de Matemáticas
Facultad de Ciencias, UNAM
Circuito Exterior, Ciudad Universitaria
México, 04510, D.F.
faustino@servidor.unam.mx

Denise Kirschner
Department of Microbiology and Immunology
6730 Medical Science Bldg II
The University of Michigan Medical School
Ann Arbor, MI 49109-0620
kirschne@umich.edu

Janelle Reynolds
Department of Oceanography
University of North Carolina
Chapel Hill, N.C. 27599
janelle@email.unc.edu